Scripta Materialia 247 (2024) 116123

Contents lists available at ScienceDirect

Scripta Materialia

journal homepage: www.journals.elsevier.com/scripta-materialia

Flash sintering can induce an anisotropic microstructure in ceramics. A phase field modeling insight

José Antonio Bejarano-Palma, Bibi Malmal Moshtaghioun *, Francisco Luis Cumbrera, Diego Gómez-García

Departamento de Física de la Materia Condensada, Universidad de Sevilla, apartado 1065, 41080 Sevilla, Spain

ARTICLE INFO

Keywords:
Anisotropy grain growth
Electric field sintering
Phase-field simulation

ABSTRACT

Field-assisted sintering techniques are at the forefront of advanced energy-saving procedures to create fully dense ceramic materials. At present, there is an extraordinary interest in understanding the sintering process and effectively controlling the final specimen's microstructure. This latter aspect is critical, but unfortunately, the short sintering times and intense electric fields under non-equilibrium conditions prevent a rigorous prediction in most cases. This paper is a theoretical contribution to gain insight into an outstanding effect of applying intense electric fields: the formation of non-spherical grain structures. A phase field simulation approach has been carried out to reproduce and determine the origin of this effect. The final simulated microstructures are proved to be textured. These results are explained in the framework of a recent model and compared with experimental evidence reported in the literature.

Field-assisted sintering techniques (FAST) for densifying nanostructured ceramics in a short time are a breakthrough for ceramists. Two important techniques have been studied intensively in this category. The first is known as spark plasma sintering (SPS), which results in improved densification thanks to a combination of pressure and high electric current density. The second, more recent, and "mysterious" ceramic processing technique is so-called flash sintering (FS), which applies a powerful electric field, resulting in sintering at significantly reduced temperature and time in comparison to traditional procedures [1–6].

On the one hand, the origin of these FAST phenomena has yet to be found and remains under debate. On the other hand, many experimental analyses have been performed to densify a wide range of ceramics. Some of them were successful, while others encountered major challenges [5–13]. An interesting feature recently observed in the careful microstructural analysis of flash-sintered ceramics is anisotropy, or, in other words, is formed by oriented elongated grains [11–13]. This important experimental observation deserves to be studied more deeply through powerful simulation techniques to gain insight into its physical phenomena. Among different methods, phase-field models are particularly useful in this context because they allow the modeling of a collective of hundreds of grains with a reasonable cost in terms of computing time. In physical terms, it is possible to model the effect of the electric field itself, with no influence from the thermal effect due to Joule heating. Such modeling is valuable and clarifying because it is practically impossible to isolate one effect from another in experiments [14].

The present work aims to investigate whether similar phenomena can also be observed in the phase-field simulation of hundreds of grains under an external electric field, which has yet to be explored. To this aim, a collective of grains with lognormal grain distribution is taken as a starting point. The standard procedure to generate such "numerical" grain microstructure is carefully described in [14]. It is important to emphasize that no porosity is assumed to occur. In addition to this, this model is not based upon the physical properties of one particular ceramic material. It is just assumed that the ceramic has a constant interfacial energy and some grain boundary conductivity, so that the grains effectively "feels" and interact with a uniform electric field.

The time evolution of a collective of grain boundaries follows the Allen-Cahn equation, which is based on the Langevin-Ginzburg-Landau one [15,16]:

$$\frac{d\eta_i}{dt} = -L_i(t)\frac{\delta F}{\delta \eta_i} \tag{1}$$

where η_i are identified as "order parameters" and describe different crystallographic orientations of grains, F is the Helmholtz free energy of

* Corresponding author.
E-mail address: mali_moshtagh@us.es (B.M. Moshtaghioun).

https://doi.org/10.1016/j.scriptamat.2024.116123
Received 14 November 2023; Received in revised form 27 February 2024; Accepted 7 April 2024
Available online 13 April 2024

a set of boundaries, and L_i is the grain mobility for each orientation i. The time evolution allows reproducing graphically a set of grains since the regions in which the order parameters have a large spatial dependence forms part of grain boundaries.

The usual expression for the Helmholtz free energy in phase-field simulations of grain growth is given by [16]:

$$f_q(\eta_1,\eta_2,\eta_3\ldots) = \sum_{i=1}^{p}\left(-\frac{\alpha}{2}\eta_i^2+\frac{\beta}{4}\eta_i^4\right)+\gamma\sum_{i=1}^{p}\sum_{j>i}^{p}\eta_i^2\eta_j^2 \tag{2}$$

$$f_\kappa(\eta_1,\eta_2,\eta_3\ldots.) = \frac{\kappa}{2}\sum_{i=1}^{p}\parallel\nabla\eta_i\parallel^2 \tag{3}$$

With

$$F = \int\int\int\left(f_q+f_\kappa\right)d^3\vec{r} \tag{4}$$

where $\alpha=\beta=\gamma=1$, $K=1/4$, $p=30$ and $t=N_S\Delta t$, where $\Delta t=0.1$. More technical details can be found in our previous paper [14]. The value of the local density of energy has been stored and used to determine the spatial energy distribution when required for analysis.

The terms in Eq. (2) forms the free energy of a collective of grains. A classical polynomial form based upon the Landau transition model is commonly adopted, in such a way that there are many local minima of the order parameters, These minima are associated to a given grain with a dominant orientation (the orientation is given by the order parameter with the smallest contribution to the free energy density. The term in Eq. (3), which depends on the gradient of the order parameter, describes the contribution of the interfacial free energy. The reader must keep in mind that, in the frame of the phase-field models, the gradients of the order parameters permit modelling "grain boundaries" [14–16].

The grain mobility L was selected to be the same for all orientations, and the constant was chosen as 0.1. One square lattice of 150 × 150 × 150 points was chosen for space discretization, periodic boundary conditions were introduced, and the Euler method was adopted for numerical integration of Eq. (1). To model the effect of an electric field, we have introduced a new term for the density of free energy, which is given by:

$$f_E(\eta_1,\eta_2,\eta_3,\ldots) = \frac{e}{2}\sum_{i=1}^{p}\left(\nabla\eta_i.\vec{E}\right)^2 \tag{5}$$

where e is a coupling constant. The value was selected as $e=1$.

This term reproduces the physical dependence of the electrostatic energy of a set of fixed charges at the grain boundaries. The gradient of the local order parameters is proportional to the surface charge density. The coupling constant would be proportional to the intrinsic conductivity of the grain boundaries [14].

The influence of different electric field intensities from 0, 0.3, 0.5 to 1 on the microstructural evolution in increasing intervals of time was studied. Our research precisely determines the non-thermal effects of an electric field in ceramic polycrystals and the induced grain growth. Periodic boundary conditions were used in all simulation tests.

Fig. 1 displays the grain size distribution as a function of the simulation time in the case of a "free specimen" (in the absence of an electric field) to analyze as a standard sample. The micrographs result from a cross-section of the specimen cut by a plane $Y=75$ (with the electric field being normal to the cross-section, namely $\vec{E}\parallel OY$) and $X=75$ (when the electric field is parallel to the cross-section along the OY direction). All micrographs have the same length scale, which allows a straightforward comparison of grain growth driven by the surface energy. The same condition has been used for all the studies under different electric field values. As expected, standard grain growth with homogeneous grain morphology was observed with progressing time. A sufficiently long time interval, in terms of simulation steps, was adopted. In our case, the interval was from 1050 to 2050 steps. After this, the electric field was removed, and the test was run for an additional 100 steps for microstructure relaxation. This allows for obtaining far more defined grain boundaries.

Fig. 2 shows the grain size distribution evolving with time for different sets of samples under several values of the external electric field from 0.3, 0.5, and 1.0 for a period of $t=1050$ to $t=2050$, followed

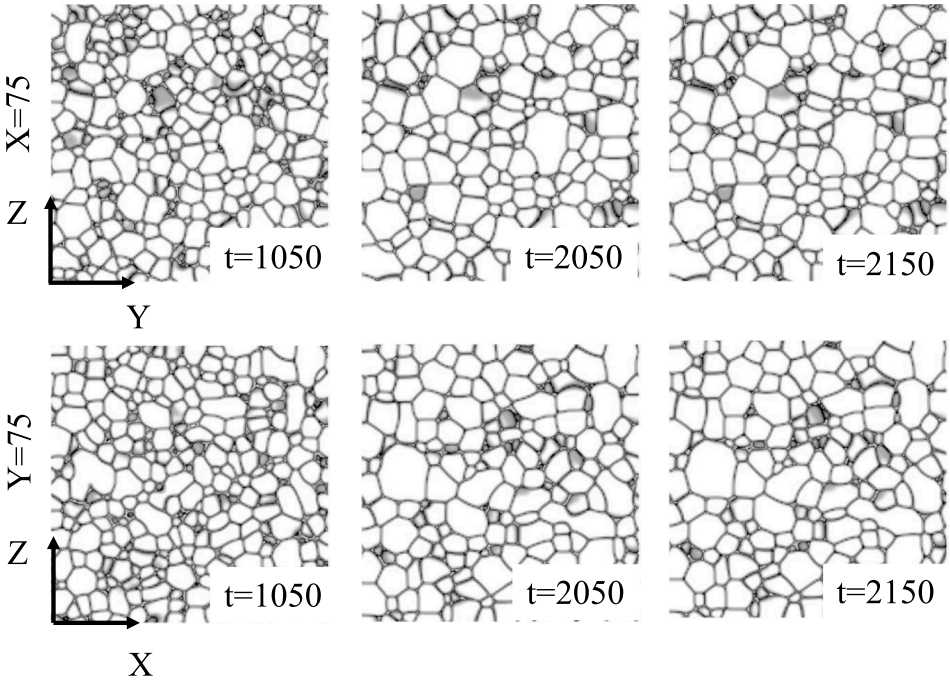

Fig. 1. Time evolution -in the absence of electric field- of the grain distribution (the cross-sections $X=75$ and $Y=25$ are displayed). The 3D phase field simulations were run with the following parameters: α = β = γ = 1.0, K = 0.25, L = 0.1, Δt = 0,1 y p = 30 [16]. The dark regions are those in which the free energy density reaches local maxima.

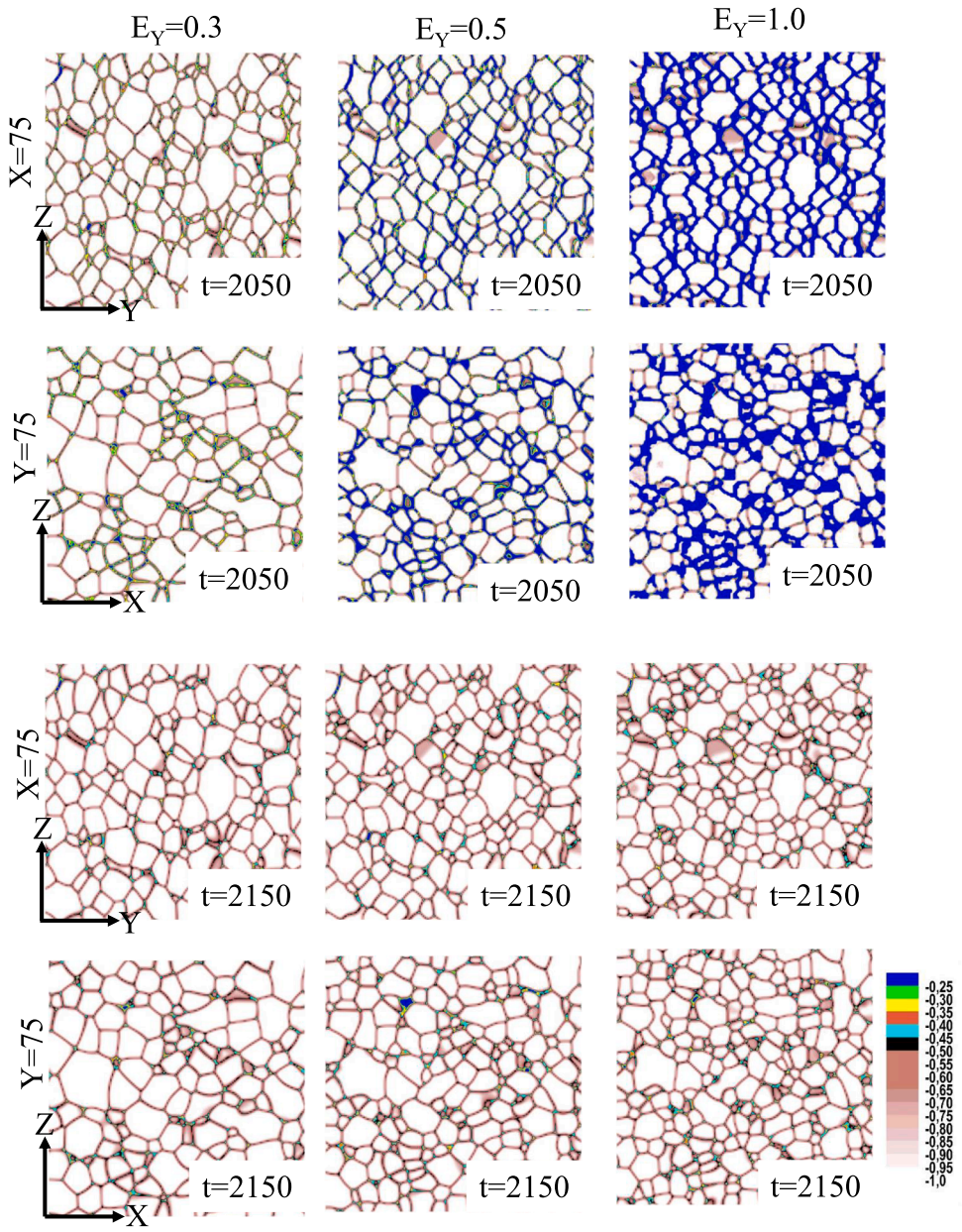

Fig. 2. Effect of the intensity of the electric field on the grain distribution. The 3D phase field simulation was carried out with the following parameters: $\alpha = \beta = \gamma = 1.0$, K = 0.25, L, $\Delta t = 0{,}1 = 0.1$ y $p = 30$ [16]. The initial state is the same for all simulations. Several values of the electric field were selected (Ey = 0.3, 0.5 and 1.0) during the time interval from $t = 1050$ until $t = 2050$ followed with a relaxation time until $t = 2150$. The grain distributions belong to $X = 75$ and $Y = 75$ cross-sections of the sample. The reader must be aware of the colour codes used to plot this figure. The regions with the minimum values of the free energy density are displayed in white or light brown colour. When the electric field increases, more and more grain boundaries are places for local energy storage. In particular, for Ey=1 many grain boundaries, in blue colour, stores a greater part of the free energy in the cross-section.

by relaxation time until $t = 2150$. The scale of local grain boundary energy densities is shown as an inset for comparison before and after the relaxation time. Please, notice that the grain boundaries can be visualized by means of a free energy density profile [14]: in other terms, the regions with grain boundaries are those with very high values of the free energy density. The code of colors provided in Fig. 2 allows observing the regions with very high values of that energy.

Several interesting features can be observed with careful analysis of the microstructure over time.

First, grain growth is hindered when the external field increases. In other words, retardation of grain growth becomes obvious with a stronger electric field. Moreover, there is a marked tendency to form clusters of small grains, which is clearer in the case of specimens under more intense electric fields. This agrees with experimental observations reported by Starners and Conrad [17] in yttria-stabilized zirconia and discussed theoretically in a previous work [14] in the following terms: when a uniform external field is applied to a spherical grain, the electrostatic pressure induced by the external electric field gives rise to a local rearrangement of electric charges at the grain surfaces, thus generating electric dipoles. Each grain behaves as an elementary dipole, contributing to the electrostatic energy density around the specimen. Energy minimization imposes that grain size should not increase because it would generate a monotonous increase in the electrostatic energy density. In simple terms, if the grain size shrinks, the intensity of the dipoles reduces proportionally. Electrostatic energy minimization determines the value of the average electrostatic pressure as opposed to

promoting grain growth [14].

The second remarkable feature is the presence of an anisotropic microstructure of non-equiaxial grains under electric field processing. This anisotropy in microstructure under different electric field intensities is well defined in a cross-section of the specimen cut by a plane $X = 75$ ($\vec{E} \| OY$). The microstructure consisted of elongated grains perpendicular to the direction of the electric field. This effect is more visible with lower electric field intensities ($E = 0.3$): the higher the electric field intensity, the finer the microstructure, and the anisotropy seems less prominent at first sight. This electric field-induced grain orientation was found experimentally in FS samples: scanning electron microscopy observations revealed grains oriented perpendicular to the electric field in specimens such as silicon carbide, alumina, and corundum [10–13], in agreement with our simulation tests. These papers suggest that the local defect arrangements due to the electrical field enhanced the diffusion kinetics by athermal effects. In other words, the orientation of the grains cannot be explained by Joule heating but through an interaction between the electric field and a mass transport mechanism [10–13].

Obviously, a homogeneous microstructure was observed in a cross-section plane of $Y = 75$, where the electric field was perpendicular to this section.

Feret diameter direction analysis was performed for all specimens. The Feret diameter can be quantified as the maximum diameter that can be drawn between any two points of the boundary of a grain. Consequently, the angle between the Feret diameter and one arbitrary fixed direction can be calculated for each grain. In our study, the fixed direction for planar section $X = 75$ was the OY direction ($\vec{E} \| OY$), and for the $Y = 75$ section, the selected direction was any radial direction perpendicular to the OY direction. The results are shown in Fig. 3 for all sets of samples at $t = 2150$ with different electric field intensities. In all figures, the dark colour histograms correspond to the case in which the electric field is orthogonal to the planar section, whereas the light colour ones are those in which the electric field is parallel to the planar section. Fig. 3A shows the case in which no electric field is applied. Both dark and light grey histogram are quite similar. Fig. 3B shows the case in which an electric field Ey=0.3 is applied. Now the yellow light colour histogram exhibits a maximum which is approximately at 90 °C from the direction of the electric field, whereas the yellow dark colour displays a uniform angular distribution. Fig. 3C shows the case in which an applied field Ey=0.5 is selected. The blue light colour distribution, the one in which the electric field is parallel to the cross-section, is clearly anisotropic: the maximum is again at one angle near 90 °C. Fig. 3D displays the case of a very intense applied electric field. This is a particular case, because the intensity of the field hinders grain growth. In total, it is confirmed that in the case of no electric field, or if one is present, for cross-sections such as $Y = 75$, the grains do not show any preferential orientation, and a flat distribution was obtained in the histogram of the relative frequency of number of grains versus the Feret angle. Conversely, an anisotropic distribution of the Feret angle is observed in the presence of an electric field for sections such as $X = 75$, indicating preferential grain growth in the plane perpendicular to the direction of the electric field. Thus, grain growth was strongly inhibited in the direction of the electric field and much less in other directions. In consequence, grains grew preferentially in a direction perpendicular to the electric field.

From a fundamental point of view, the atomistic explanation of grain growth inhibition can be understood in the frame of a recently reported model [14]. The anisotropic effect can be explained as follows: the inhibition of grain growth is driven by the electrostatic pressure induced

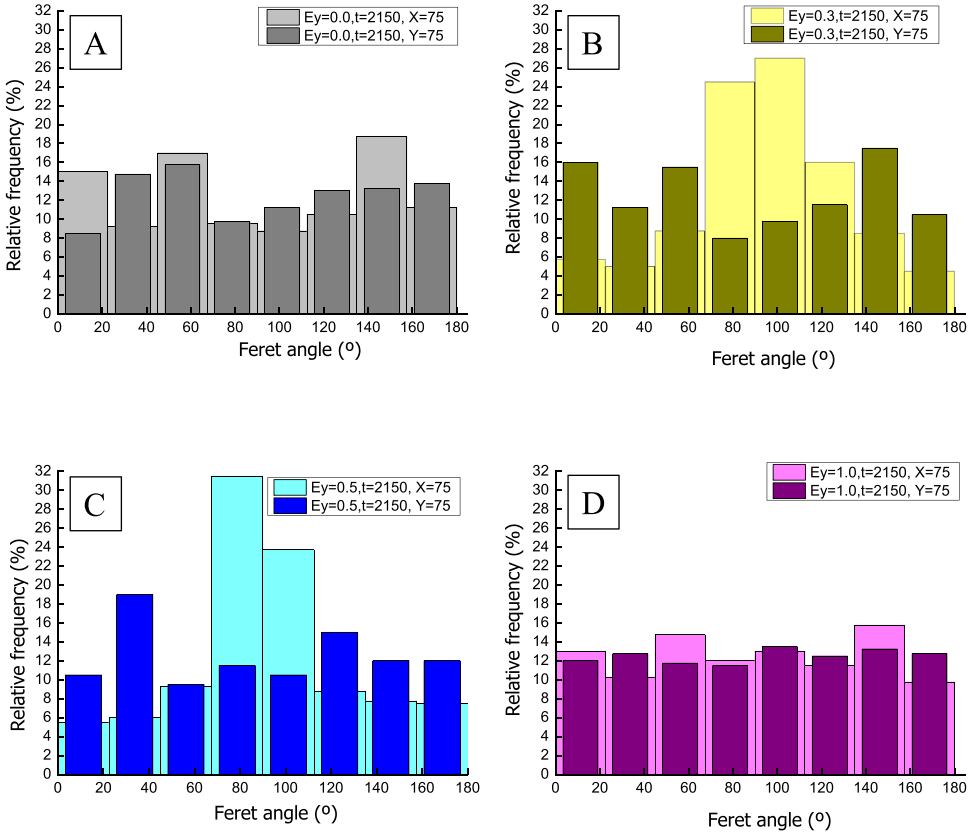

Fig. 3. Histogram of the relative frequencies (percentage of number of grains per angle interval) as a function of Feret angle in grain distributions obtained from $X = 75$ and $Y = 75$ cross-section of the sample at $t = 2150$ for (A) no electric field Ey=0.0, (B) an applied electric field: Ey=0.3 (C) an applied electric field: Ey=0.5 and (D) a very intense applied electric field: Ey=1.0 . In all figures, the dark colour histograms correspond to the case in which the electric field is orthogonal to the planar section, whereas the light colour ones are those in which the electric field is parallel to the planar section.

by the applied external electric field. Such pressure is proportional to E_n^2, E_n being the normal component of the electric field, i.e., the one perpendicular to the grain surface. The grain can be described approximately like a sphere, $E_n^2 \simeq E^2\cos\theta$, where θ is the angle between the direction of the electric field and the vector normal to the surface. If we select the direction of the electric field as the reference direction to calculate the Feret angle, θ will be exactly that angle. Taking these considerations into account, the contribution of the electric field to limiting grain growth will be zero if $\theta=\pi/2$ and maximized when $\theta=0$.

Therefore, grains tend to grow perpendicular to the applied electric field, whereas grain growth is minimal parallel to the applied electric field.

The microstructure is logically affected by this source of anisotropy. There is a way to prove the consistency of this statement. Electric pressure can be considered as an energy barrier to be overcome for grains to grow, which reaches its maximum value when $\theta=0$ and decreases to zero when $\theta=\pi/2$. If the grain boundaries have high enough mobilities, the probability of encountering a grain oriented along a given direction, θ, must follow the general Maxwell-Boltzmann distribution, i.e.:

$$P(\theta)\propto\exp\left(\frac{-aE^2\cos^2\theta}{kT}\right) \tag{6}$$

The frequencies (f) of the different orientations must be proportional to $P(\theta)$. If we normalized their values so that $f = 1$ when the grains are oriented along the electric field (θ=1), then the proportionality constant is determined trivially:

$$f(\theta) = \exp\left[-a\frac{E^2}{kT}\left(\cos^2\theta - 1\right)\right] = \exp\left(a\frac{E^2}{kT}\sin^2\theta\right) \tag{7}$$

The constant a depends on the material under study, and kT has its usual meaning in physics. Notice that if a is known, it is possible to determine the actual value of the electric field inducing anisotropy at a given temperature T. The relative number of grains versus the angle θ must fit into a Gaussian distribution of the variable $\cos\theta$. This is displayed in Fig. 4, in which the relative frequency of grains is plotted versus $\cos\theta$ for $E = 0.3$ and $E = 0.5$. As commented above, the frequencies have been rescaled for normalization to a value of one when the grains are oriented along the electric field. Fig. 4 reveals several interesting observations: First, all results fit into a Gaussian distribution with high accuracy (the correlation factor is higher than 0.92 for $E = 0.3$ and higher than 0.98 for $E = 0.5$, even if grains are not exactly spheres). Second, the Gaussian distribution is wider for the $E = 0.3$ test and narrower for the $E = 0.5$ one, as expected from the mathematical dependence depicted in Eq. (7). This indirect analysis is consistent with the physical basis of this problem: grains behave as "electrostatic dipoles," inducing spatial orientation, while grain boundary energy creates growth in all directions (statistical randomness). Contrary to classical statistical physics models, such as the Langevin model, the preferred orientation is not along the electric field but perpendicular to it.

From a practical point of view, the actual values of electric fields that could induce an anisotropic microstructure largely depend on the values of the electrostatic pressure (in our case, the constant a shown in Eq. (7)). According to the results reported in [14], electric fields as high as 10^5 V/m are required for yttria-zirconia. Such fields can be present in advanced sintering techniques like flash sintering. This opens a new way to develop ceramic materials with preferential directions.

Conclusions

We conducted phase field simulations of electric-field-driven grain growth and its effect on remarkable anisotropic microstructure. The simulated microstructure is realistic, showing grain growth induced and oriented by the external field. Grain growth is controlled by the tendency of the grains to grow preferentially perpendicular to the electric field, resulting in enlarged grains, therefore an anisotropic microstructure. The formation of such microstructures had been invoked in literature but for the first time this phenomenon is explained in terms of the orientational dependence of electric field pressure, which determines the grain growth kinetics. An analytical model based upon statistical physics is proposed, and it agrees with the simulation outputs. It is demonstrated that grains behave as "electrostatic dipoles," inducing spatial orientation, while grain boundary energy creates growth in all directions. Contrary to classical statistical physics models, such as the Langevin model, the preferred orientation is not along the electric field but the normal one. The paper proves the importance of strong-electric-field-induced sintering techniques. This paper proves that electric-field assisted techniques can be used to prepare ceramics with an anisotropic microstructure composed of elongated grains for potential applications on demand.

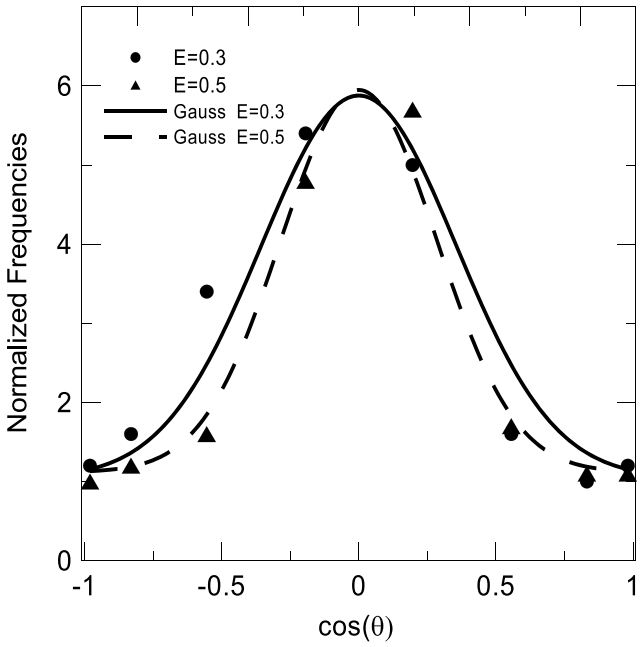

Fig. 4. Relative frequencies versus cosθ, (θ being the Feret angle) for the $E = 0.3$ and $E = 0.5$ simulation tests. The Feret angles were determined from snapshots taken from $X = 75$ cross-sections. The frequencies have normalized, meaning that the value one is chosen for $\theta=0$, and the others are scaled proportionally. The continuous line is the best fitting to a gaussian function for the values of $E = 0.3$, whereas the dashed lines are the corresponding similar fitting for the values of $E = 0.5$. the correlation factors are $r = 0.92$ and $r = 0.98$, respectively. The analysis is not made for simulation test with $E = 1$, because the measurement of the frequencies versus the Feret angle is less accurate. This is connected to the fact the width (w) of the gaussian function decreases as $w\propto 1/E^2$.

Declaration of competing interest

The authors declare that they have no known competing financial interests or personal relationships that could have appeared to influence the work reported in this paper.

Acknowledgments

The authors acknowledge the financial support provided by the Agencia Española de Investigación through the grant PID2019-103847-RJ-100 funding by MCIN/AEI/10.13039/501100011033.

References

[1] M. Rahaman, Ceramic Processing and Sintering, Marcel Dekker, 1995.

[2] S. Grasso, Y. Sakka, G. Maizza, Electric current activated/assisted sintering (ECAS): a review of patents 1906–2008, Sci. Technol. Adv. Mater. 10 (2009) 53001.
[3] O. Guillon, J. Gonzalez-Julian, B. Dargatz, T. Kessel, G. Schierning, J. Räthel, M. Herrmann, Field-assisted sintering technology/spark plasma sintering: mechanisms, materials, and technology developments, Adv. Eng. Mater. 16 (2014) 830–849.
[4] M. Biesuz, V.M. Sglavo, Flash sintering of ceramics, J. Eur. Ceram. Soc. 39 (2019) 115–143.
[5] M. Yu, S. Grasso, R. Mckinnon, T. Saunders, M.J. Reece, Review of flash sintering: materials, mechanisms and modelling, Adv. Appl. Ceram. 116 (2017) 24–60.
[6] K. Naik, S.K. Jha, R. Raj, Correlations between conductivity, electroluminescence and flash sintering, Scr. Mater. 118 (2016) 1–4.
[7] R.I. Todd, E. Zapata-Solvas, R.S. Bonilla, T. Sneddon, P.R. Wilshaw, Electrical characteristics of flash sintering: thermal runaway of Joule heating, J. Eur. Ceram. Soc. 35 (2015) 1865–1877.
[8] J. Janek, C. Korte, Electrochemical blackening of yttria-stabilized zirconia – morphological instability of the moving reaction front, Solid State Ion. 116 (1999) 181–195.
[9] M. Biesuz, P. Luchi, A. Quaranta, V.M. Sglavo, Theoretical and phenomenological analogies between flash sintering and dielectric breakdown in α-alumina, J. Appl. Phys. 120 (2016) 145107.
[10] A. Gibson, Y. Li, R.S. Bonilla, R.I. Todd, Pressureless flash sintering of α-SiC: electrical characteristics and densification, Acta. Mater. 241 (2022) 118362.
[11] S. Grasso, E.-Y. Kim, Th. Saunders, M. Yu, A. Tudball, Sh-H. Choi, M. Reece, Ultra-rapid crystal growth of textured SiC using flash spark plasma sintering route, Cryst. Grow. Des. 16 (2016) 2317–2321.
[12] Ch. Shen, T. Niu, B. Yang, J. Cho, Z. Shang, T. Sun, A. Shang, R.E. García, H. Wang, X. Zhang, Micromechanical properties and microstructures of AC and DC flash-sintered alumina, Mater. Sci. Eng. A 866 (2023) 144631.
[13] M. Biesuz, V.M. Sglavo, Current-induced abnormal and oriented grain growth in corundum upon flash sintering, Scripta Mater. 150 (2018) 82–86.
[14] J.A. Bejarano-Palma, B.M. Moshtaghioun, F.L. Cumbrera, D. Gómez-García, On the role of the electric field in fast sintering of ceramics; a phase field approach, Acta. Mater. 262 (2024) 119422.
[15] L. Q.Chen, Phase-field models for microstructure evolution, Annu. Rev. Mater.Res 32 (2002) 113–140.
[16] L.Q. Chen, W. Yang, Computer simulation of the domain dynamics of a quenched system with a large number of non-conserved order parameters: the grain-growth kinetics, Phys. Rev. B 50 (1994) 15752–15756.
[17] S. Starners, H. Conrad, Grain size distribution in ultrafine-grained yttria-stabilized zirconia deformed without and with an electric field, Scripta Mater. 59 (2008) 1115–1118.